MATHEMATICAL MODELING
OF
ANNULAR REACTORS

Mark E. Davis

Layne T. Watson

CS84003-R

ABSTRACT

A generalized mathematical model for describing the whole-cell-hollow-fiber reactor and the annular bed reactor is presented. The annular reactor model consists of a mixed-type problem for which a novel numerical procedure is developed. The procedure is demonstrated for a number of examples, and it is proved that the model and solution technique are well suited for the simulation of annular reactors.

INTRODUCTION

In recent years two reactors of analogous configuration have been theoretically and experimentally studied, and show promise. These two reactors are the whole-cell hollow-fiber reactor (WCFR) [1-4], and the annular bed reactor (ABR) [5-8]. Each reactor is made up of a central core which is surrounded by an annular region of catalytically active material (see Figure 1). For the WCFR the active material is whole-cells, and for the ABR it is solid catalyst. In the WCFR, the two regions are separated by the hollow-fiber wall, and in the ABR they are kept apart by an inert screen.

The purpose of the WCFR design is to immobilize the catalytically active, enzymatic material by immobilizing the whole-cells. Advantages of immobilizing whole-cells over that of enzymes are [2]: minimization of enzyme denaturation, elimination of enzyme purification, and the ability of whole cells to catalyze multistep reactions.

The ABR is configured such that for highly exothermic reactions, the reactor shows good thermal behavior. This advantage of the ABR has been experimentally confirmed using the hydrogenation of benzene with a supported nickel catalyst as the test reaction [8]. Ultimate uses for the ABR could include systems which involve supported transition metal catalysts, and reactions which produce coke. Supported transition metal catalysts are very sensitive to temperature, and thus require excellent temperature control. In the case of a coking reaction, the coke formation would occur in the annulus and could never plug the core,

where the regenerative oxygen flows. Therefore, regeneration, a highly exothermic reaction, could not be inhibited by tube plugging due to coke formation as it is with fixed-bed reactors.

Although these two reactors have been designed for different purposes, their structure is the same, and thus they can be described by similar sets of mathematical relationships. In this paper we (a) develop a generalized mathematical model for these annular reactors, (b) introduce a new computational procedure for solving models of the structure given in (a), and (c) show the feasibility of the computational procedure for modeling the WCFR and the ABR.

REACTOR MODEL

The following reactor model is developed to describe annular reactors in general, and thus can be used to simulate the WCFR and the ABR. Simplified versions of this model have been previously derived by other investigators [2-6, 8, 9].

Consider a mixture of MT chemical species which participate in MR independent chemical reactions:

$$\sum_{n=1}^{MR} \nu_{n,q} A_n = 0, \qquad q = 1, \ldots, MR.$$

Assuming that the effects of volume changes due to the reactions on the concentrations and axial velocity can be neglected, the continuity balances for the inert core are:

$$uV(r)\frac{\partial C_n}{\partial z} = \frac{D_n^c}{r}\frac{\partial}{\partial r}\left(E(r)r\frac{\partial C_n}{\partial r}\right), \qquad n = 1, \ldots, MR, \tag{1}$$

$$uV(r)\rho C_p\frac{\partial T}{\partial z} = \frac{K^c}{r}\frac{\partial}{\partial r}\left(G(r)r\frac{\partial T}{\partial r}\right), \tag{2}$$

for $0 \le r \le r_s$, $0 \le z \le L$, with

$$\frac{\partial C_n}{\partial r} = 0 \text{ at } r = 0, \quad D_n^c E(r_s^-)\left.\frac{\partial C_n}{\partial r}\right|_{r_s^-} = D_n^s\left.\frac{\partial C_n}{\partial r}\right|_{r_s^+} \text{ at } r = r_s, \; n=1,\ldots,MR, \tag{3}$$

$$\frac{\partial T}{\partial r} = 0 \text{ at } r = 0, \quad K^c G(r_s^-)\left.\frac{\partial T}{\partial r}\right|_{r_s^-} = K^s\left.\frac{\partial T}{\partial r}\right|_{r_s^+} \text{ at } r = r_s, \tag{4}$$

and

$$C_n = C_n^o \text{ for } n = 1, \ldots, MR, \qquad T = T^o \text{ at } z = 0. \tag{5}$$

The radial distribution functions are included to allow for point transport coefficients and for laminar or turbulent velocity profiles. The functionality of V(r), E(r), and G(r) for turbulent flow in the ABR is described elsewhere [6]. If $V(r) = E(r) = G(r) = 1$ for $0 \le r \le r_s$, then the traditional turbulent flat velocity and dispersion profiles are obtained. Also, if $E(r) = G(r) = 1$ and $V(r) = 2\left[1 - (r/r_s)^2\right]$ for $0 \le r \le r_s$, the traditional laminar velocity and diffusion coefficients are acquired. In Eqs. (2) and (3) axial dispersion processes are

neglected. This omission may not be applicable for certain cases in the ABR [7], but in the majority of the anticipated uses for the ABR and the WCFR, the neglecting of axial dispersion effects is justified.

The continuity balances for the medium which separates the inert core and the active bed (membrane or screen) are:

$$\frac{D_n^s}{r}\frac{\partial}{\partial r}\left(r\frac{\partial C_n}{\partial r}\right)=0, \qquad n=1,\ \ldots\ ,\ MR, \tag{6}$$

$$\frac{K^s}{r}\frac{\partial}{\partial r}\left(r\frac{\partial T}{\partial r}\right)=0, \tag{7}$$

for $r_s \leq r \leq r_b$, with

$$D_n^c E(r_s^-)\left.\frac{\partial C_n}{\partial r}\right|_{r_s^-} = D_n^s \left.\frac{\partial C_n}{\partial r}\right|_{r_s^+} \text{ at } r=r_s,\quad D_n^s \left.\frac{\partial C_n}{\partial r}\right|_{r_b^-} = D_n^b \left.\frac{\partial C_n}{\partial r}\right|_{r_b^+} \text{ at } r=r_b, \tag{8}$$

$$n=1,\ \ldots\ ,\ MR,$$

$$K^c \left.\frac{\partial T}{\partial r}\right|_{r_s^-} = K^s \left.\frac{\partial T}{\partial r}\right|_{r_s^+} \text{ at } r=r_s,\quad K^s \left.\frac{\partial T}{\partial r}\right|_{r_b^-} = K^b \left.\frac{\partial T}{\partial r}\right|_{r_b^+} \text{ at } r=r_b. \tag{9}$$

Finally, the continuity balances for the active bed are:

$$\frac{D_n^b}{r}\frac{\partial}{\partial r}\left(r\frac{\partial C_n}{\partial r}\right)=\sum_{q=1}^{MR}\nu_{n,q}R_q, \qquad n=1,\ \ldots\ ,\ MR, \tag{10}$$

$$\frac{K^b}{r}\frac{\partial}{\partial r}\left(r\frac{\partial T}{\partial r}\right) = \sum_{q=1}^{MR} \Delta H_q R_q, \tag{11}$$

for $r_b \leq r \leq r_o$, with

$$D_n^s \left.\frac{\partial C_n}{\partial r}\right|_{r_b^-} = D_n^b \left.\frac{\partial C_n}{\partial r}\right|_{r_b^+} \text{ at } r = r_b, \quad \frac{\partial C_n}{\partial r} = 0 \text{ at } r = r_o, \quad n=1,\ldots,MR, \tag{12}$$

$$K^s \left.\frac{\partial T}{\partial r}\right|_{r_b^-} = K^b \left.\frac{\partial T}{\partial r}\right|_{r_b^+} \text{ at } r = r_b, \quad K^b \frac{\partial T}{\partial r} = \overline{U}(T - T^o) \text{ at } r = r_o. \tag{13}$$

For the ABR, r_o designates the inside surface of the reactor tube wall, while in the case of the WCFR it represents the so called "hollow fiber mid-point" [2]. The hollow fiber mid-point is calculated by equating the total cell suspension volume to that of the individual annulus volume multiplied by the number of hollow fibers in the unit. Examples of this calculation are given in [2-4]. A proper simplification of Eq. (13) when describing the WCFR is to set $\overline{U} = 0$; that is, zero heat transfer occurs across the hollow fiber mid-point. (For most practical situations, the WCFR will be essentially isothermal and the addition of the heat balance not required.)

COMPUTATIONAL TECHNIQUES

A nonlinear, mixed-type problem similar to that described by Eqs. (1-13) has been previously solved by a non-iterative finite difference

method [5-7]. This procedure involved an extrapolated Crank-Nicolson discretization, and details can be found elsewhere [9].

For thick catalytic beds, near complete conversion within the catalytic region is possible at any z. Although computed concentrations must remain finite at $r = r_o$ (except for zero-order reaction rate, see Appendix A), they can become exceedingly small for significant portions of the active bed. In this case, the procedure given in [9] requires excessively small meshes in both the axial (due to extrapolation), and radial (due to truncation error) directions. Next, we develop a new computational procedure which overcomes this difficulty and can be used for all problems with structure similar to that of Eqs. (1-13).

To begin, the core balances, which are of parabolic type, are discretized. For the purpose of illustration, we outline the procedure on a single equation, with $V(r) = E(r) = 1$. Let $y_{i,j}$ denote the approximation to the exact solution $C_n(i\Delta r, j\Delta z)$ for grid points $i = 0, \ldots, N$, $j = 0, 1 \ldots M$, where $\Delta r = r_s/N$ and $\Delta z = L/M$. A Crank-Nicolson discretization of Eq. (1) is:

$$\left[1 + \frac{2\Delta z\, D_n^c}{u(\Delta r)^2}\right] y_{0,j+1} - \frac{2\Delta z\, D_n^c}{u(\Delta r)^2}\,(y_{1,j} + y_{1,j+1}) + \left[\frac{2\Delta z\, D_n^c}{u(\Delta r)^2} - 1\right] y_{0,j} = 0, \qquad (14)$$

$$\frac{\Delta z\, D_n^c}{2u(\Delta r)^2}\left[\left(1 + \frac{1}{2i}\right)\left(y_{i+1,j+1} + y_{i+1,j}\right) + \left(1 - \frac{1}{2i}\right)\left(y_{i-1,j+1} + y_{i-1,j}\right)\right] +$$

$$\left[1 - \frac{\Delta z\, D_n^c}{u(\Delta r)^2}\right] y_{i,j} - \left[1 + \frac{\Delta z\, D_n^c}{u(\Delta r)^2}\right] y_{i,j+1} = 0, \quad i = 1, \ldots, N-1. \qquad (15)$$

Next, approximate the flux at r_s by

$$D_n^c \left.\frac{\partial C_n}{\partial r}\right|_{r_s^-} \simeq \frac{D_n^c}{2\Delta r} (y_{N-2,j+1} - 4y_{N-1,j+1} + 3y_{N,j+1}). \tag{16}$$

Since the screen or membrane continuity balance is easily integrated, the "jump" across this region is accomplished using Eq. (16) to give:

$$C_n(r_b) \simeq \frac{r_s D_n^c}{2\Delta r D_n^s} (y_{N-2,j+1} - 4y_{N-1,j+1} + 3y_{N,j+1}) \operatorname{Ln}\left(\frac{r_b}{r_s}\right) + y_{N,j+1}, \tag{17}$$

$$\left.\frac{\partial C_n}{\partial r}\right|_{r_b^+} \simeq \frac{r_s D_n^c}{2\Delta r\, r_b D_n^b} (y_{N-2,j+1} - 4y_{N-1,j+1} + 3y_{N,j+1}). \tag{18}$$

Equations (17) and (18) together with Eq. (10) (for a given n) constitute an initial value problem for the active bed. A variable order, variable step Adams method is used to solve the ordinary differential equation until $r = r_o$ or $C_n = 0$, whichever occurs first. The remaining boundary condition which must be satisfied is

$$\left.\frac{\partial C_n}{\partial r}\right|_{r_o} = 0 \qquad \text{if} \qquad C_n(r_o) \geq 0, \tag{19}$$

or

$$\left.\frac{\partial C_n}{\partial r}\right|_{\bar{r}} = 0 \qquad \text{if} \qquad C_n(\bar{r}) = 0, \quad r_b \leq \bar{r} < r_o. \tag{20}$$

Appendix A proves that the boundary condition $C_n(\bar{r}) = \left.\frac{\partial C_n}{\partial r}\right|_{\bar{r}} = 0$ is impossible except for a zero-order reaction rate. Thus, Eq. (12) is ultimately satisfied for all non-zero-order reaction rates. Equation (20) is included to explain how the numerical algorithm handles the case where $C_n(r_o) < 0$. The boundary value problem within the bed is known as a "free boundary" problem. Note that the value of $\left.\frac{\partial C_n}{\partial r}\right|_{r_o}$ or $\left.\frac{\partial C_n}{\partial r}\right|_{\bar{r}}$ depends in a highly nonlinear and implicit fashion on the values of the core concentrations $y_{i,j+1}$, $i = 0, \ldots, N$. Conversely, the free boundary condition in the bed propagates inward and implicitly imposes a constraint on the solution in the core. Thus, Eqs. (14), (15), (19) and (20) comprise a set of N+1 nonlinear equations in the N+1 unknowns $y_{i,j+1}$, $i = 0, \ldots, N$.

The nonlinear system of equations is solved for each z-level by a least change secant update quasi-Newton algorithm [10]. Since the concentration varies slowly, obtaining good starting points for the quasi-Newton iteration poses no difficulty. Furthermore, the slow variation of the concentration and the small band width of the Jacobian matrix makes the quasi-Newton iteration very efficient.

The error in the numerical solution is a combination of several factors. These are: (a) error in discretizing the parabolic core equations (Eqs. (14) and (15)), (b) error in approximating the flux at r_s (Eq. (16)), (c) error from the variable order, variable step Adams method used to solve the active bed equations, and (d) the error

associated with the least change secant update quasi-Newton algorithm. The expected core discretization error is $O(\Delta z^2 + \Delta r^2)$ where $O(\ )$ denotes terms of order ( ); that is, $f(\Delta z) = O(\Delta z^{\xi})$ if $|f(\Delta z)| \leq \Phi(\Delta z)^{\xi}$ as $\Delta z \to 0$ (ξ and Φ are constants) [11]. The error in approximating the flux at r_s is $O(\Delta r^2)$ while the errors associated with the Adams method and the quasi-Newton are determined by specifying their magnitudes, and are denoted by TOLA and TOLN respectively.

NUMERICAL EXPERIMENTS

To show its feasibility, the computational method proposed is demonstrated for three subcases of the generalized reactor model. All calculations have been performed on a VAX 11/780 in double precision arithmetic. Example 1 shows the computational properties, e.g., approximation errors, quasi-Newton iterations, of the method. Examples 2 and 3 illustrate the use of the reactor model and computational procedure to describe a liquid-phase reaction system in the WCFR (single species) and a gas-phase reaction system in the ABR (two species), respectively. The final two examples demonstrate that the model and numerical procedure are sufficient to simulate gas or liquid phase reaction systems over a wide range of operating conditions.

EXAMPLE 1

Consider a fictitious annular reactor where $r_s = r_b$, that is, no screen or membrane is required to separate the inert core from the active bed. Also, assume that the reactor is isothermal and that a reaction

with a zero-order reaction rate is occurring in the active bed. If the concentration of the reactant remains positive at r_o, then the effectiveness factor for the catalytically active bed is equal to one [2, 3]. Thus, the annular reactor can be described by (E(r) = 1):

$$2u\left[1 - \left(\frac{r}{r_s}\right)^2\right]\frac{\partial C_1}{\partial z} = D_1^c\left[\frac{\partial^2 C_1}{\partial r^2} + \frac{1}{r}\frac{\partial C_1}{\partial r}\right], \quad 0 \leq r \leq r_s, \quad 0 \leq z \leq L, \tag{21}$$

with

$$\frac{\partial C_1}{\partial r} = 0 \text{ at } r = 0, \qquad D_1^c\frac{\partial C_1}{\partial r} = \bar{k} \text{ at } r = r_s,$$

and

$$C_1 = C_1^o \text{ at } z = 0,$$

where

$$\bar{k} = -\left[\frac{r_o^2 - r_s^2}{2r_s}\right]k.$$

The analytical solution to Eq. (21) is (converted from the heat transfer analog [12]):

$$\frac{C_1\left(\frac{r}{r_s}, z\right) - C_1^o}{(\bar{k}r_s/D_1^c)} = \frac{2z\,D_1^c}{ur_s^2} + \frac{11}{24} + \sum_{\ell=1}^{\infty}\psi_\ell R_\ell\left(\frac{r}{r_s}\right)\exp\left[\frac{-\beta_\ell^2 z\,D_1^c}{2ur_o^2}\right], \tag{22}$$

where the first seven values of ψ, $R(1)$, and β^2 are given in Table 1. Now let $r_s = 1$, $r_o = 1.5$, $D_1^c = 0.1$, $D_1^s = 0.1$, $D_1^b = 0.1$, $u = 10$, $C_1^o = 1\times10^{-5}$, and $k = 1\times10^{-6}$. Using the above parameters, Eq. (22) gives $C_1(1, z)$ to at least five significant figures for $\ell \geq 3$.

The reactor model consists of Eqs. (1), (3), (5), (6), (8), (10), and (12) with MR = 1, $\nu_{1,1} = 1$, and $R_1 = k$. Provided the reactant concentration remains finite at r_o, the numerical solutions are independent of the magnitudes of D_1^s and D_1^b as predicted by Eq. (22). Table 2 shows the root mean square error (RMSE) in the numerical solution for various Δr and Δz. The RMSE is defined as:

$$\text{RMSE} = \sqrt{\sum_{j=1}^{M} \frac{(C_1(1,j\Delta z) - y_{N,j})^2}{M}} \quad .$$

From these results, the numerical procedure is shown to be consistent with the differential equation model. That is, RMSE $\rightarrow$ 0 as Δr and $\Delta z \rightarrow 0$. For the results given in Table 2, the average number of function calls is seven. (One function call represents one evaluation of the system of nonlinear equations.) The minimum possible number of function calls per j-step is seven. Thus, increasing TOLN will not aid in increasing speed. When TOLN was set below 10^{-6} there was no change in the RMSE, but the execution time increased due to the larger number of function calls required to obtain the higher accuracy. For values of TOLA $< 10^{-6}$, the RMSE was not changed from those reported in Table 2, while execution times increased slightly with tighter TOLAS.

From the above discussion it becomes clear that the major source of error is the core discretization which is coupled to the error in approximating the flux at r_s. Although the finite difference method outlined in this paper is the easiest discretization (especially for the case of multiple equations with $E(r) \neq 1$, $G(r) \neq 1$), Galerkin and collocation procedures are recommended if higher accuracy is desired. For complete discussions on Galerkin and collocation refer to Chapters 3 and 4 of [11].

Figure 2 shows the axial dimensionless profiles at the centerline, the core-bed interface, and at the outer surface of the bed. The differences between pairs of curves indicate the overall concentration gradients between corresponding boundaries. This figure also shows, for $z/L > \sim 0.2$, the concentration gradients in the two regions are of approximately equal magnitude. Thus, the highly coupled nature of the system is well illustrated by this example.

EXAMPLE 2

Webster and Shuler [4] describe the following experiment. A WCFR with physical dimensions listed in Table 3 contains a mutant cell slurry with a high concentration of the enzyme urease. A urea substrate solution at a concentration of 2.00 g/ℓ is pumped through the reactor at an everage velocity of 2.235 cm/s. It was observed that the urea concentration exiting the WCFR was 1.80 g/ℓ. It is known that the diffusivity of urea in water and in the hollow fiber membrane is 1.2×10^{-5} cm^2/s [14], and 1.63×10^{-6} cm^2/s [4], respectively. Given

that the first-order reaction rate constant is 0.01125 s^{-1}, the desired quantity is the diffusivity of urea in the mutant cell slurry.

Webster and Shuler [4] considered their reactor to be operating differentially, and neglected the diffusion resistance of the core in their analysis. Thus, the concentration in the core was assumed uniform for all r and z. Their results specified $D_1^b = 1.2 \times 10^{-5}$ cm^2/s; the same value for that of urea is pure water. Although the mutant cell slurry could contain a high concentration of water, it is very unlikely that the diffusivity of urea through this slurry would be equal to that in pure water.

We modeled this reactor system using Eqs. (1), (3), (5), (6), (8), (10) and (12) with MR = 1, $E(r) = 1$, $V(r) = 2\left[1 - (r/r_s)^2\right]$, $\nu_{1,1} = 1$, and $R_1 = 0.01125\ C_1$. In order to obtain the specified outlet average concentration, we found that $D_1^b = 3.0 \times 10^{-7}$ cm^2/s. Figure 3 shows the radial concentration profiles for various axial positions when using $D_1^b = 3.0 \times 10^{-7}$ cm^2/s. As can be seen from Figure 3, the concentration is not uniform for $0 \leq r \leq r_s$, $0 \leq z \leq L$, and this effect produces a two order of magnitude difference in the calculated values of D_1^b. Our value of D_1^b appears more reasonable in light of the magnitude of the urea diffusivity in pure water, and a complete discussion the physical implications of this result will be presented elsewhere [13]. The primary conclusion drawn from using the full model is that the major diffusion resistance is the whole-cell slurry, and not the hollow-fiber membrane as reported by Wester and Shuler.

EXAMPLE 3

Davis et al. [8] hydrogenated benzene over a supported nickel catalyst in an ABR. The stoichometry of the reaction is:

$$C_6H_6 + 3H_2 = C_6H_{12}.$$

It was found that

$$R_1 = \frac{838T^2 \exp\left[\frac{7,326}{T}\right] C_1 C_2}{1 + 1.96\times10^{-6} T \exp\left[\frac{68,768}{T}\right] C_1} \left(\frac{\text{gmoles}}{\text{cm}^3\cdot\text{s}}\right) \qquad (23)$$

where C_1 and C_2 are the concentration of benzene and hydrogen, respectively. Because of the hydrogen dependence in R_1, hydrogen material balances are needed for the solution of the benzene continuity equations. Since there is only one independent reaction, the hydrogen balances can be obtained as follows. In the inert core, the flow is turbulent for this case, and transport will be dominated by convective processes. Thus, $D_2^c E(r) = D_1^c E(r)$, and

$$C_2 = C_2^o - 3(C_1^o - C_1), \qquad 0 \le z \le L,\ 0 \le r \le r_s. \qquad (24)$$

Since it is assumed that no axial flow occurs in the screen and catalytic bed, transport in these regions is purely molecular in nature. Therefore, the hydrogen continuity balances for the screen and catalytic bed are respectively:

$$C_2 = C_2(r_s) - 3\left(\frac{D_1^s}{D_2^s}\right)\left[C_1(r_s) - C_1\right], \qquad r_s \leq r \leq r_b, \tag{25}$$

where $C_2(r_s)$ is calculated from Eq. (24), and

$$C_2 = C_2(r_b) - 3\left(\frac{D_1^b}{D_2^b}\right)\left[C_1(r_b) - C_1\right], \qquad r_b \leq r \leq r_o, \tag{26}$$

where $C_2(r_b)$ is computed with Eq. (9). In total, the reactor model consists of Eqs. (1-13, 23-26) with MR = 1 and $\nu_{1,1} = 1$.

Parameter data representative of the ABR in our laboratory are given in Table 4. The results of simulating the ABR with the data listed in Table 4 are shown in Figures 4 and 5. For this set of data, the model calculated the exit conversion of benzene to be 93%. As can be seen in Figure 4, the reactor model predicted relatively small temperature gradients. These results illustrate the excellent thermal behavior of the ABR. Figure 5 shows the concentration profiles in the forward and exit regions of the reactor. As can be seen in Figure 5, the magnitude of the concentration gradient decreases with increasing axial position.

The results provided in Figures 4 and 5 show that the numerical procedure can adequately "handle" problems which contain large gradients, gradients in opposing directions (gradient always negative for concentration, but changes sign in various regions for temperature), and multiple continuity balances.

CONCLUSIONS

The results presented herein demonstrate the effectiveness of the annular reactor model and its associated solution technique for the simulation of annular reactors in general.

REFERENCES

[1] Kan, J. K., and M. L. Shuler, Biotechnol. Bioeng., 20, 217 (1978).

[2] Webster, I. A., and M. L. Shuler, Biotechnol. Bioeng., 20, 1541 (1978).

[3] Webster, I. A., M. L. Shuler, and P. R. Rony, Biotechnol. Bioeng., 21, 1725 (1979).

[4] Webster, I. A., and M. L. Shuler, J. Chem. Tech. Biotechnol., 31, 226 (1981).

[5] Davis, M. E., G. Fairweather, and J. Yamanis, Can. J. Chem. Eng., 59, 497 (1981).

[6] Davis, M. E., and J. Yamanis, A.I.Ch.E.J., 28, 266 (1982).

[7] Davis, M. E., and J. Yamanis, Chem. Eng. Commun., 25, 1 (1984).

[8] Davis, M. E., N. Bungard, M. D. Burnett, E. Hawkins, L. T. Watson, and J. Yamanis, Inst. Chem. Eng. Symp. Ser., No. 87, xxx (1984).

[9] Fairweather, G., M. E. Davis, and J. Yamanis, Chem. Eng. Commun., 23, 89 (1983).

[10] Watson, C. T., and C. Y. Wang, Int. J. Solids Structures, 17, 29 (1981).

[11] Davis, M. E., Numerical Methods and Modeling for Chemical Engineers, John Wiley and Sons, New York (1984).

[12] Siegel, R., E. M. Sparrow, and T. M. Hallman, Appl. Sci. Res. Sec. A., 7, 386 (1958).

[13] Davis, M. E., and L. T. Watson, in preparation.

[14] Shampine, L. F., and M. K. Gordon, Computer Solution of Ordinary Differential Equations, W. H. Freeman, San Francisco (1975).

[15] DeBruijn, E. W., W. A. DeJong, and T. Van Der Speigel, ACS Sym. Ser., No. 65, 63 (1978).

NOTATION

A	reaction component
C_n	concentration of species n
C_p	heat capacity
D_n^c, D_n^s, D_n^b	diffusivity of species n in the core, screen, and bed
$E(r)$	distribution function for radial mass dispersion
$G(r)$	distribution function for radial heat dispersion
ΔH_q	heat of reaction for the q^{th} reaction
k	zero-order reaction rate constant
K^c, K^s, K^b	thermal conductivity in the core, screen, and bed
L	reactor length
MT	total number of species in the system
r	radial corrdinate
R_q	reaction rate function for the q^{th} reaction
R	parameter in Eq. (22)
u	average axial velocity
$\overline{U}$	overall heat transfer coefficient
$V(r)$	radial distribution function for axial velocity
$y_{i,j}$	numerical approximation to $C(i\Delta r, j\Delta z)$
z	axial coordinate

Greek Symbols

β	parameter in Eq. (22)
$\nu_{i,j}$	stoichiometric coefficient of i for the j reaction

ρ	density
ψ	parameter in Eq. (22)

Subscripts

s	at core-screen interface
b	at screen-bed interface
o	at wall or hollow fiber mid-point

Superscripts

c	in the core region
s	in the screen or membrane region
b	in the bed region
o	at the reactor inlet
+	evaluated from the outer side of the interface
-	evaluated from the inner side of the interface

APPENDIX A

Zero-Order Kinetics

The equations describing the annular catalytic region are ordinary differential equations (ODEs). More specifically, the ODEs are two-point boundary-value problems with highly implicit and nonlinear boundary values at $r = r_b$, and satisfy the boundary condition of $dC/dr = 0$ with C remaining positive at r_o. For certain forms of the reaction rate function, "reactant exhaustion" occurs, and the conditions at r_o are replaced by $C = dC/dr = 0$ at $\bar{r}$ where $r_b \leq \bar{r} < r_o$. Below we show that the form of the reaction rate function determines whether "reactant exhaustion" conditions are appropriate substitutions for the standard boundary conditions in an annular reactor.

Consider the following ODE which can describe the behavior of the catalytically active bed

$$\frac{d^2C}{dr^2} + \frac{1}{r}\frac{dC}{dr} = R(C), \tag{A.1}$$

and write it as a first-order system:

$$\begin{aligned} \frac{d\alpha_1}{dr} &= \alpha_2, \\ \frac{d\alpha_2}{dr} &= R(\alpha_1) - \frac{\alpha_2}{r} \end{aligned} \tag{A.2}$$

where $\alpha_1 = C$ and $\alpha_2 = dC/dr$. Now let $r_b \leq \bar{r} \leq r_o$. Invoking the "reactant exhaustion" conditions at $\bar{r}$ as initial conditions for (A.2), and integrating to $r = r_b$ gives $C = 0$ at r_b except for the case where $R(C=0) \neq 0$. In other words, if $C \equiv 0$ satisfies (A.1) then it is the only solution to (A.1) (see [14] for an existence and uniqueness proof for solution to (A.2)). Since C at r_b is not zero (no reaction in core and screen), "reactant exhaustion" can not occur for a R(C) that satisfied $R(C=0) = 0$. Thus, for $R(C=0) = 0$, the boundary condition $dC/dr = 0$ with C remaining positive at r_o must be satisfied. Alternatively, if $R(C=0) \neq 0$, then "reactant exhaustion" can occur. Such is the case when $R(C) = k$, or zero-order kinetics.

DeBruijn et al. [15] modeled their parallel passage reactor (rectangular coordinate analog of the annular reactors) by specifying $C = dC/dr = 0$ at $r = r_o$. Since their reactor model satisfied $R(C=0) = 0$, the "reactant exhaustion" condition is mathematically impossible, and calculations based on it are at best accidentally correct if $dC/dr(r_o) = 0$ and $C(r_o) \approx 0$, or at worst just plain wrong.

TABLE HEADINGS

Table 1: Parameter Values for Equation (22) from Reference [12].

Table 2: Root Mean Square Error in the Numerical Solution. TOLA = TOLN = 10^{-6}.

Table 3: Whole-Cell-Hollow-Fiber Reactor Data from Reference [4].

Table 4: Annular Bed Reactor Data.

FIGURE LEGENDS

Figure 1: Schematic of Whole-Cell-Hollow-Fiber or Annular Bed Reactor. Laminar velocity distribution function is illustrated.

Figure 2: Axial dimensionless concentration profiles.

Figure 3: Radial concentration profiles in the whole-cell-hollow-fiber reactor with $D_1^b = 2.0 \times 10^{-7}$ cm^2/s. Core (I), membrane (II), and whole-cells (III).

Figure 4: Temperature Contours in the ABR.

Figure 5: Radial Dimensionless Concentrations in the ABR.

Table 1

ℓ	β_ℓ^2	$R_\ell(1)$	ψ_ℓ
1	25.6796	-0.492517	0.403483
2	83.8618	0.395508	-0.175111
3	174.167	-0.345872	0.105594
4	296.536	0.314047	-0.0732804
5	450.947	-0.291252	0.0550357
6	637.387	0.273808	-0.043483
7	855.850	-0.259852	0.035597

Table 2

$(\Delta z, \Delta r)$	RMSE
0.025 , 0.1000	0.2187×10^{-1}
0.025 , 0.0500	0.7791×10^{-2}
0.025 , 0.0250	0.4508×10^{-2}
0.100 , 0.0125	0.4350×10^{-2}
0.050 , 0.0125	0.4076×10^{-2}
0.0250, 0.0125	0.3937×10^{-2}

Table 3

Parameter	Value
r_s	0.01001 cm
r_b	0.01300 cm
r_o	0.01781 cm
L	21 cm

Table 4

Parameter	Value
u	20.35 cm/s
D_1^c	6.105 cm^2/s
D_1^c/D_2^c	1.0
D_1^s	0.447 cm^2/s
D_1^s/D_2^s	1.0
D_1^b	0.447 cm^2/s
D_1^b/D_2^b	1.0
ρC_p	2.27×10^{-4} cal/cm^3-K
K^c	1.39×10^{-3} cal/cm-s-K
K^s	2.48×10^{-2} cal/cm-s-K
K^b	1.25×10^{-3} cal/cm-s-K
r_s	0.8484 cm
r_b	0.8712 cm
r_o	1.27 cm
L	15.54 cm
$E(r) = V(r) = G(r) = 1.0$	----
$\overline{U}$	5.98×10^{-3} cal/cm^2-s-K
T^o	390 K
C_1^o	5.34×10^{-7} gmole/cm^3
C_1^o/C_H^o	0.0174
ΔH	-50,000 cal/gmole

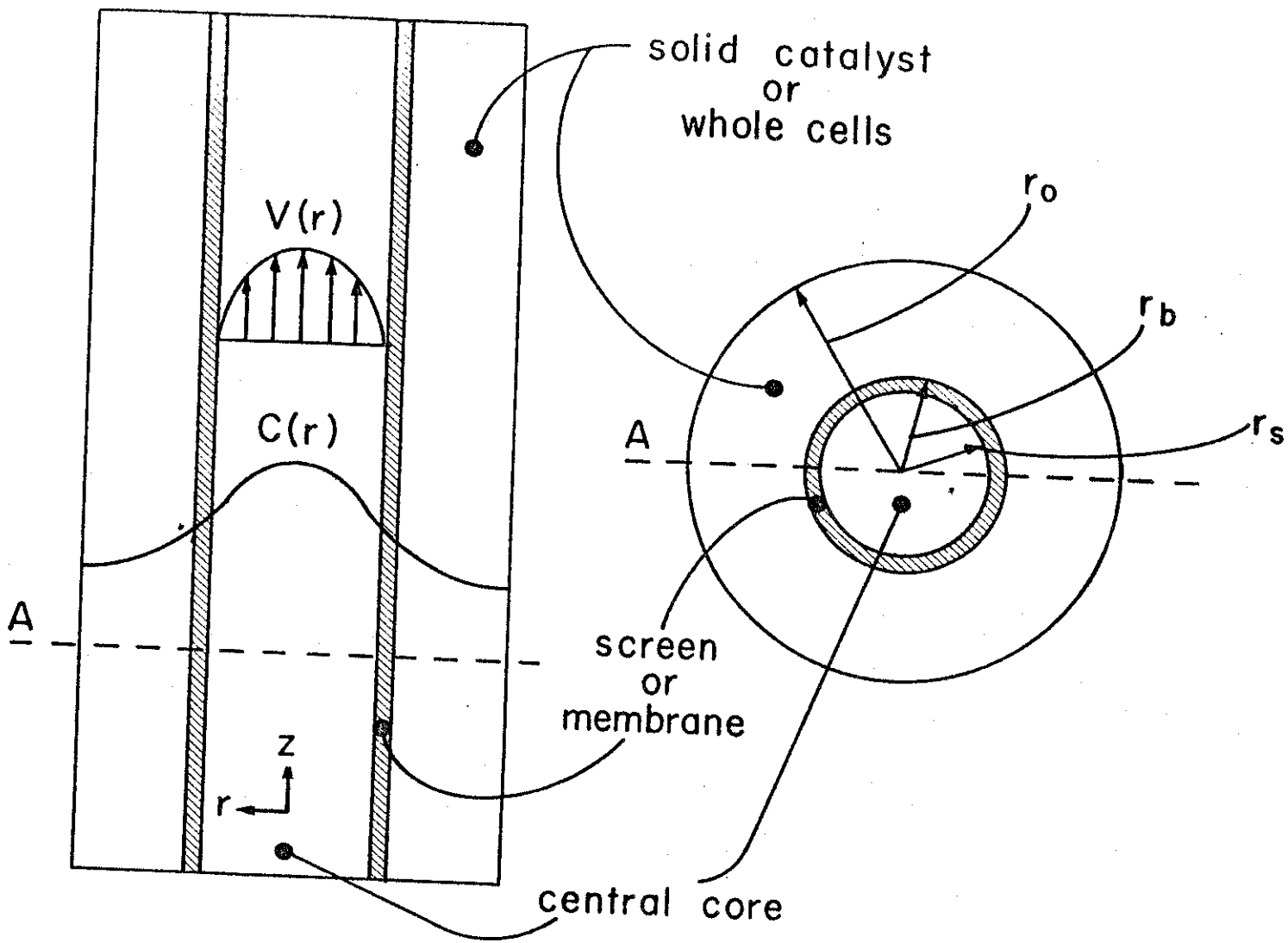
solid catalyst
or
whole cells
V(r)
C(r)
A
A
screen
or
membrane
z
r
central core
r_o
r_b
r_s

Fig. 1

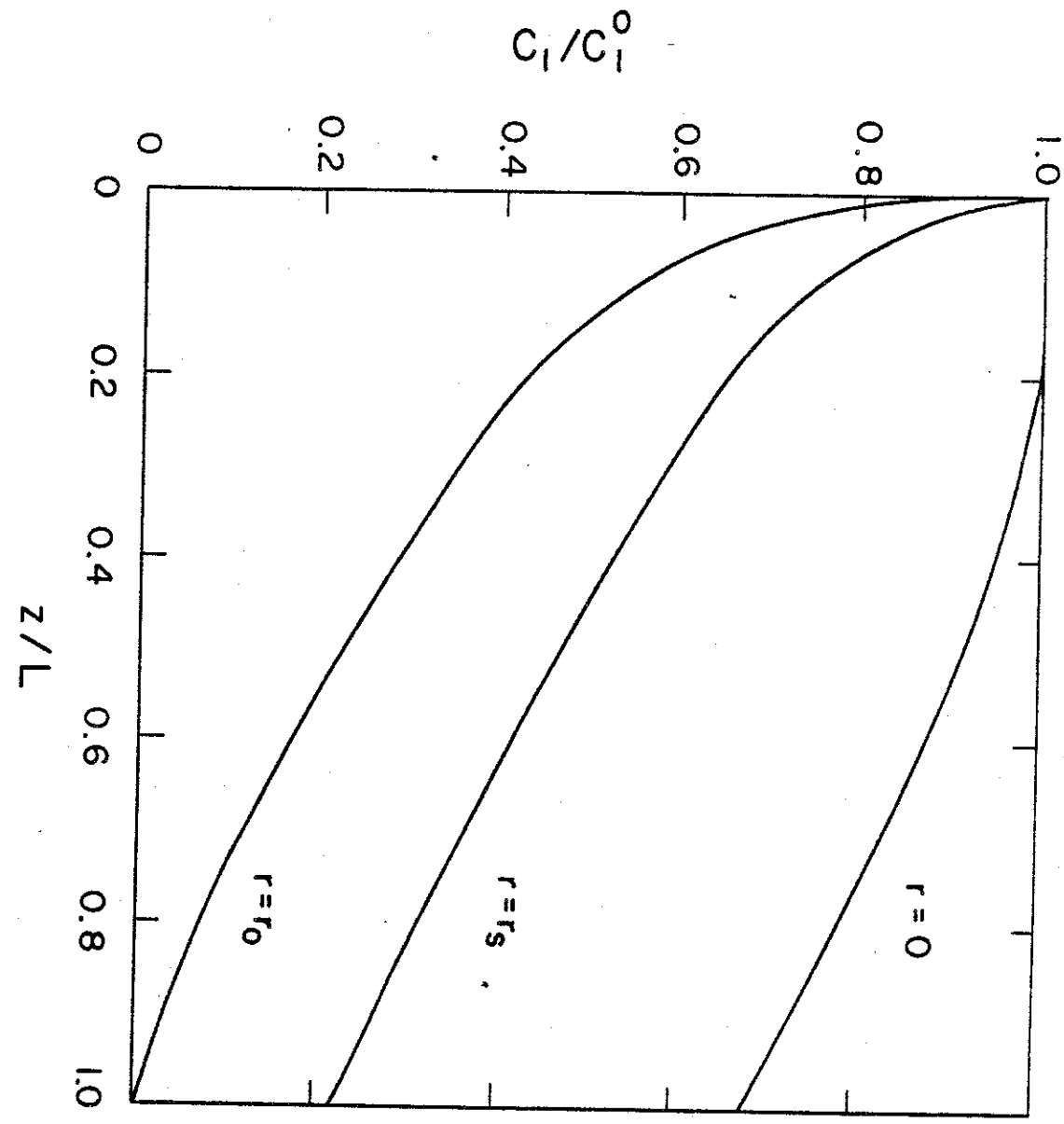

Fig. 2

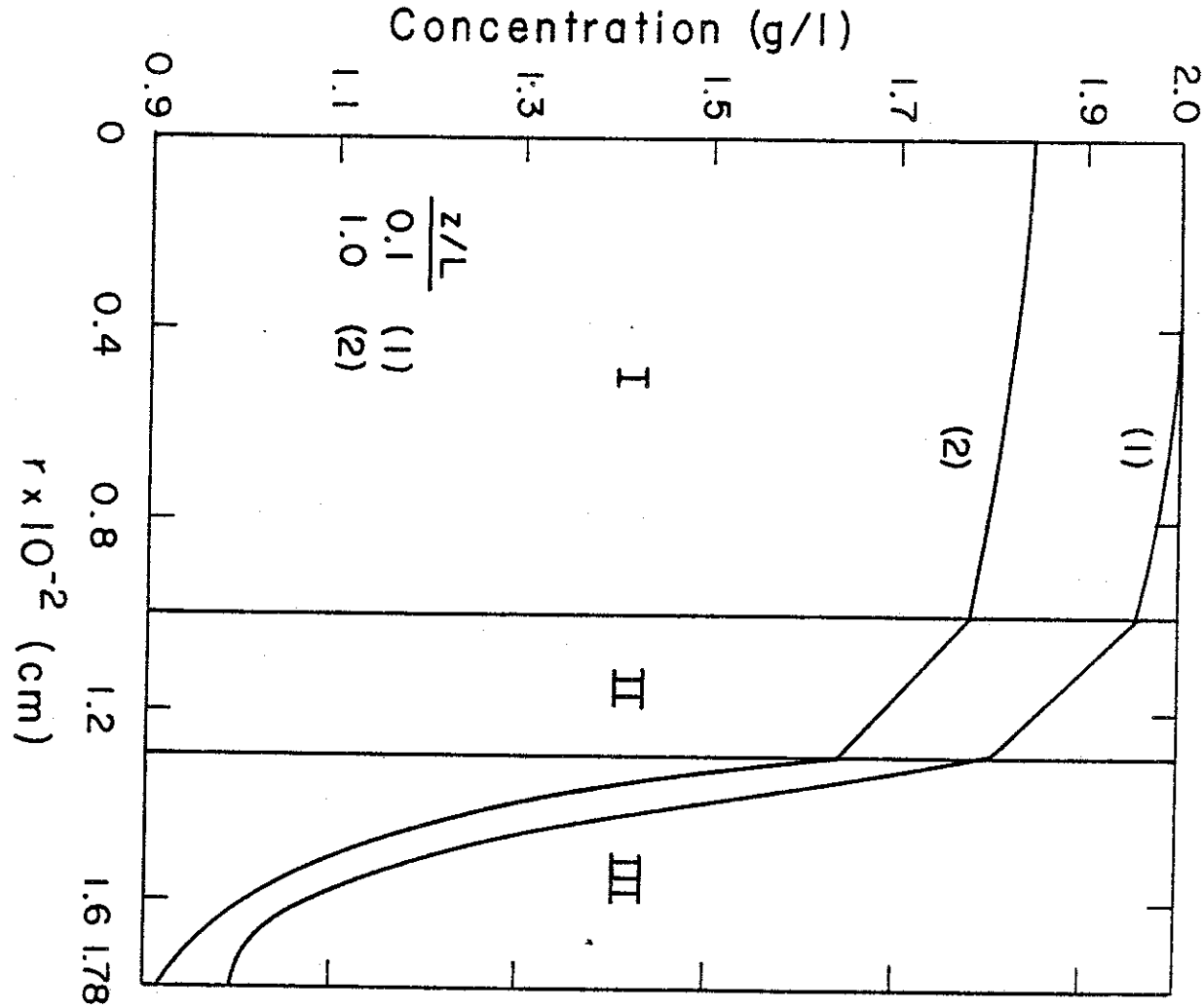
Concentration (g/l)
0.9
1.1
1.3
1.5
1.7
1.9
2.0
0
0.4
0.8
1.2
1.6
1.78
r x 10-2 (cm)
z/L
0.1
1.0
(1)
(2)
I
II
III
(2)
(1)

Fig. 3

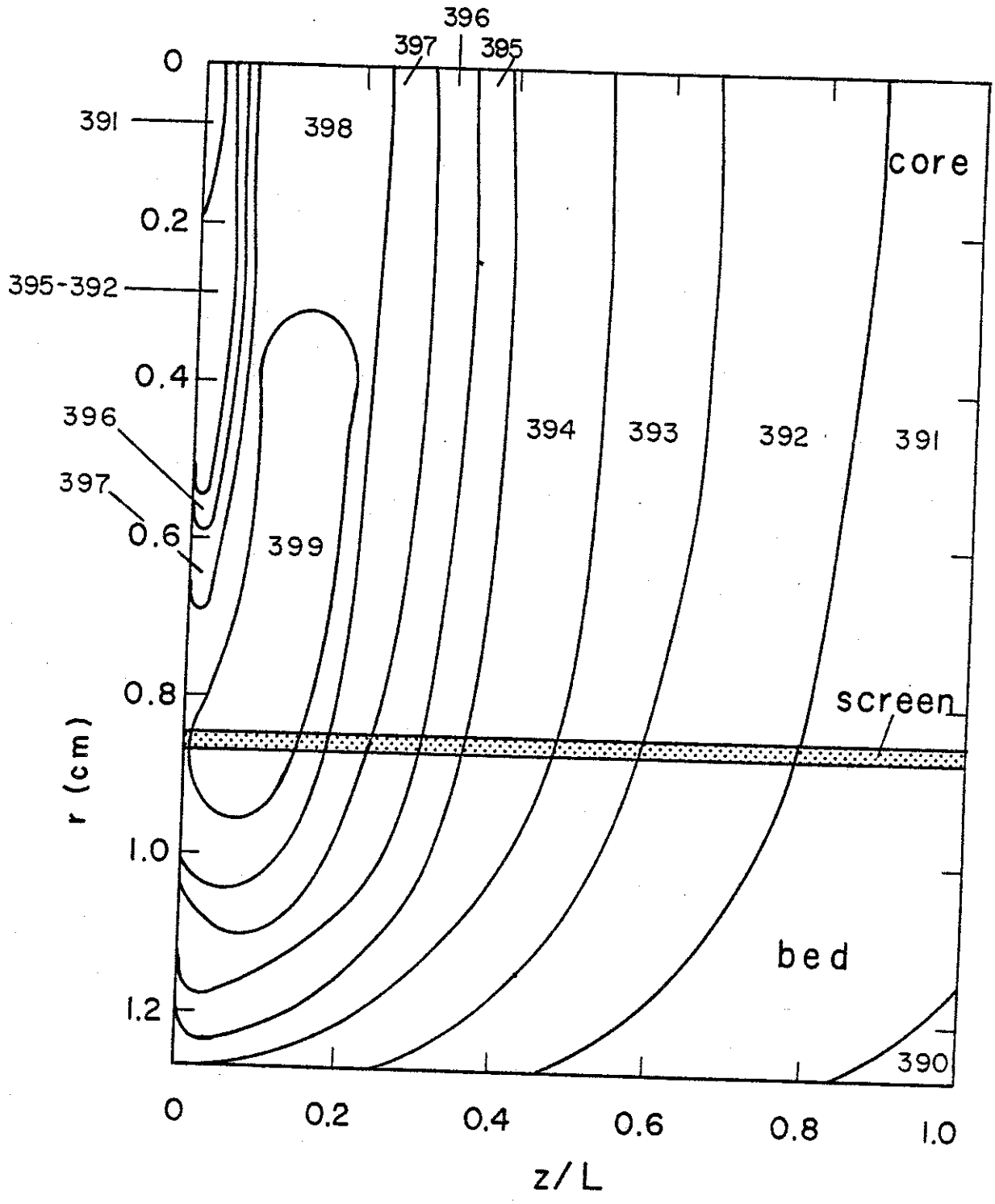
396
397
385
0
391
398
core
0.2
395-392
0.4
396
394
393
392
391
397
0.6
399
0.8
screen
r (cm)
1.0
bed
1.2
390
0
0.2
0.4
0.6
0.8
1.0
z/L

Fig. 4

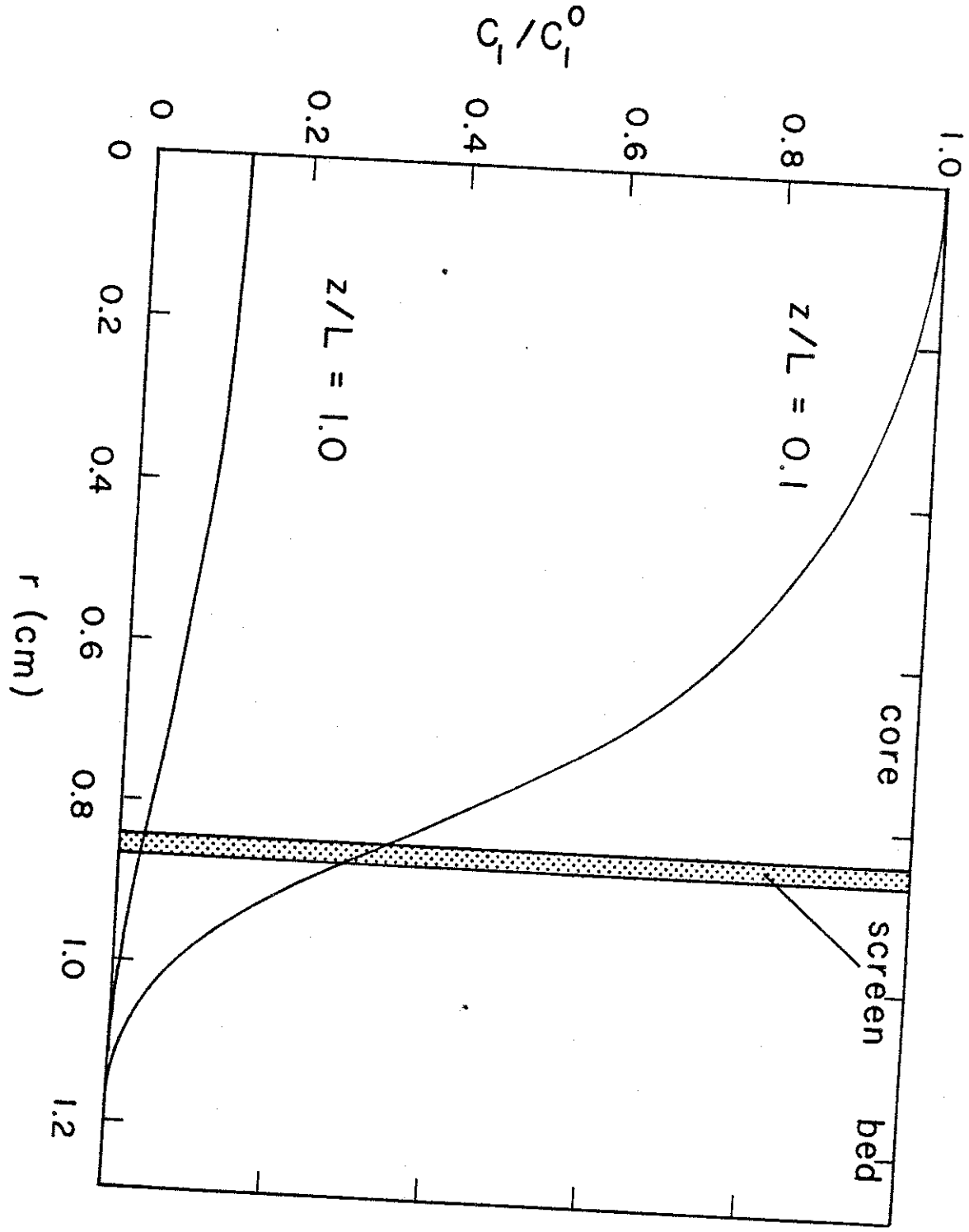
C_1 / C_1^o
0
0.2
0.4
0.6
0.8
1.0
r (cm)
0.2
0.4
0.6
0.8
1.0
1.2
z/L = 1.0
z/L = 0.1
core
screen
bed

Fig. 5